Aluminium self diffusion in high-purity α-Al_2O_3: Comparison of Ti-doped and undoped single crystals

Peter Fielitz[1*], Steffen Ganschow[2], Klemens Kelm[3], Günter Borchardt[1]

[1] Technische Universität Clausthal, Institut für Metallurgie, Robert-Koch-Str. 42, D-38678 Clausthal-Zellerfeld, Germany

[2] Leibniz-Institut für Kristallzüchtung, Max-Born-Str. 2, D-12489 Berlin, Germany

[3] Deutsches Zentrum für Luft- und Raumfahrt, Institut für Werkstoff-Forschung, Linder Höhe, D-51147 Köln, Germany

* corresponding author: e-mail: peter.fielitz@tu-clausthal.de

Abstract

Reliable data on self diffusion of aluminium in α-Al_2O_3 are scarce and do not yet enable deriving quantitative conclusions about the impact of deliberate aliovalent doping. Therefore, the present study ($1280 \le T/°C \le 1500$, $p_{O2} = 200$ mbar) was based on carefully grown high-purity single crystals doped with Ti. The experimentally determined ^{26}Al tracer diffusivity increased with the Ti concentration and confirmed the incorporation of Ti on Al sites, $Ti_{Al}^{\bullet}$, with aluminium vacancies, V_{Al}''', formed for charge compensation. The observed relation between these two point defect concentrations as a function of the Ti concentration and the temperature can be quantitatively modelled by taking into account probable $Ti_{Al}^{\bullet} : V_{Al}'''$ clusters. Using binding energy starting values from published computer simulations for the fit procedure cluster binding energies are obtained. The surprisingly high Al diffusivity in undoped samples can be tentatively rationalised by injection of Al interstitials at the liquid/solid interface because of the low oxygen potential during the crystal growth process.

Key words: alumina; Ti-doped; tracer diffusion; ^{26}Al; SIMS; defect clusters

1 Introduction

Beside its role in optoelectronics α-Al_2O_3 is an important refractory material which has numerous technical applications: as an in situ growing self-healing oxide scale, as a massive material and as reinforcement fibres in composites. The formation of a protective α-Al_2O_3 scale is a crucial requirement for high-temperature Al-containing alloys (for instance FeCrAl and NiCrAl) to resist oxidation under their operating conditions [1],[2]. Just as oxide scale growth, sintering, creep, and grain growth depend strongly on diffusion processes [3]-[5]. In 2011 Heuer et al. [2] compiled the best available bulk diffusivity data for oxygen and aluminium in Al_2O_3. In this compilation there is a striking discrepancy between the amount of data for the diffusion of oxygen (7 data sets) as compared to the diffusion of aluminium (2 data sets). The reason for the dearth of data for aluminium is that this element has only one stable isotope (^{27}Al). The only radionuclide (^{26}Al) which can be used for diffusion measurements is very expensive and difficult to handle [6]-[8].

Considering the available published aluminium diffusion data there is a remarkable agreement between the data published by Paladino and Kingery [9] in 1962 and those published by Fielitz et al. [10] in 2008. This agreement is in fact surprising because Paladino and Kingery used nominally *undoped* samples (polycrystalline, 96 % of theoretical density, grain size 100–200 µm), whereas Fielitz et al. used *Ti-doped* samples (single crystalline, 300-400 wt ppm Ti-doped). Due to the rather large grain size and due to the temperature range of their experiments it is plausible that Paladino and Kingery measured the bulk diffusion coefficient of aluminium in these samples. For Mg, Ca, Fe, Mn, and Si concentrations were determined in the order of less than about 100 ppm by spectrographic analysis [9].

In 2008 Fielitz et al. [10] assumed (in accordance with, e.g., conductivity measurements of Mohapatra and Kröger [11]) that tetravalent titanium ions, Ti^{4+}, occupy aluminium sites and that Al vacancies, V_{Al}''', rather than oxygen interstitials, O_i'', are the majority defects, which

yields the simple electroneutrality condition $[Ti_{Al}^{\bullet}]-3[V_{Al}''']\cong 0$ if the formation of defect clusters is neglected. That is, in undoped crystals one could assume a significantly lower Al diffusivity than in 300-400 wt ppm Ti-doped crystals. To verify this assumption Fielitz et al. [12] in 2012 measured ^{26}Al diffusivities in *undoped* α-Al_2O_3 single crystals. The result was very surprising because there was almost no difference of the ^{26}Al tracer diffusivity in the undoped and in the Ti-doped single crystals of that study.

In the light of the contradictory data the present study was primarily designed to (re)investigate the dependence of the aluminium diffusion in single crystalline α-Al_2O_3 on Ti doping. In order to enable a reliable interpretation of the diffusion data it was an absolutely crucial requirement to dispose of single crystals which virtually differ solely by the dopant concentration. In order to fulfil this requirement a close cooperation between experienced crystal growers (Leibniz Institute for Crystal Growth, Berlin, Germany) had been established which guaranteed that all of the crystals were grown in the same Czochralski system, using identical starting powders for the melts.

The second objective was to scrutinize current concepts on defect interactions in doped α-Al_2O_3.

2 Experimental Procedures

2.1 Crystal growth and doping

Single crystals were grown using the Czochralski technique with induction heating. The starting material consisting of premelted granules of Al_2O_3 (Spolchemie, ~5N purity) doped with appropriate amounts of TiO_2, was melted in a 40 ml cylindrical iridium crucible. An active afterheater was placed on top of the crucible to create above the melt a thermal cavity into which the crystal was pulled. The crucible/afterheater arrangement was enclosed in alumina and zirconia ceramic elements for additional thermal insulation.

All crystals were grown on identical seeds from pure Al_2O_3 oriented along the a-axis. Crystal pulling rate and rotation were adapted to the dopant level in the melt. Additionally, to reduce the risk of interface break-down due to constitutional supercooling, the pulling rate was decreased by a factor of two from the top to the bottom of the cylindrical crystal part with constant diameter of 18 mm. The undoped reference crystal and crystals with low dopant concentration were pulled with a starting rate of 2.0 mm/h, while for those with highest dopant concentration the initial rate was 0.5 mm/h. To intensify melt mixing, crystal rotation was simultaneously increased from 10 to 20 rpm.

Knowledge of the solute segregation coefficient is essential to pull crystals with desired dopant concentration. Regarding the titanium distribution coefficient in sapphire there is, unfortunately, some ambiguity [13]-[15]. The observable dopant distribution in a grown crystal is caused by an effective distribution coefficient that is strongly affected by growth conditions, in particular growth velocity and melt mixing, e.g. by convection. Moreover, oxygen activity in the growth unit greatly impacts the chemical equilibrium between the various titanium oxidation states. At oxygen activities typically achieved in contemporary melt growth equipment $\left(\log(a_{O_2}) \approx -6\right)$, titanium will exist mainly in the 3^+ state. It has been shown [16] that when pulling ruby ($Cr^{3+}:Al_2O_3$) crystals the overall distribution of chromium can be controlled via the relative amounts of different chromium species, in that case Cr^{2+} and Cr^{3+}. The analogous phenomenon must be expected to have a significant influence on the Ti distribution coefficient.

Table 1 Planned and analysed Ti dopant concentrations of the single crystals grown for this investigation.

planned [wt ppm Ti]	300	600	900	1200
ICP [wt ppm Ti]	263 ± 5	593 ± 10	1010 ± 20	1100 ± 20

Previous experiments [10] yielded an effective Ti distribution coefficient of 0.05 for growth conditions similar to those applied during this study. This value is significantly lower than

reported by other authors for a strongly reducing environment [15],[17]. Table 1 shows that regarding the distribution coefficient given above the achieved Ti concentrations in the crystals were nearly on target.

Chemical element analysis of the Ti-doped samples was carried out using an inductively coupled plasma (ICP) spectrometer IRIS Intrepid HR Duo (Thermo Elemental, USA). The spectrometer was calibrated with simple synthetic solution standards with matrix correction. Fragments of the samples were ball-milled, dissolved in a microwave heated mixture of phosphoric and sulphuric acid at 250 °C and analysed [18]. The solutions were also checked for Zr and Fe, the two most probable impurities that might originate from the growth process, as the thermal insulation consisted partially of zirconia ceramics. Both element concentrations were below the detection limit (ca. 5 ppm for Fe and ca. 10 ppm for Zr).

Table 2 Concentration (wt ppm) of elements which are above the detection limit of a GDMS analysis in an undoped and in a Ti-doped α-Al_2O_3 single crystal.

	B	Na	Mg	Si	P	S	Cl	K	Ca	Ti	Cr
undoped	0.09	0.53	0.08	1.4	2.6	2.3	0.53	1.1	1.1	< 0.05	< 0.5
Ti-doped	0.07	0.47	0.63	1.9	3.4	1.3	0.63	1.0	1.1	580	< 0.5

To get an overview of all impurities Glow Discharge Mass Spectrometry (GDMS) was used which provides sensitivity at the sub-ppm level for almost all elements in the periodic table [19]. A full scan GDMS analysis (Evans Analytical Group SAS, Toulouse, France) includes 75 elements (except C, N, O, H). The detection limit is in the range from 0.01 to 0.5 wt ppm (except Fe < 1, Ge < 1, Nb < 50, Mo < 20, W < 20 wt ppm). Concentrations of impurities in an undoped and in a Ti-doped α-Al_2O_3 single crystal which are above the detection limit of the GDMS analysis are listed in Table 2. We see that the detectable impurities (B, Na, Mg, Si, P, S, Cl, K, Ca, Cr) are similar in both samples and practically not influenced by the doping of the single crystals.

2.2 TEM analysis

Transmission electron microscopy (TEM) investigations were carried out on ion-beam thinned samples. For this, 3 mm discs were drilled from flat triangular single crystal plates of three samples which were doped with 593 ppm or 1100 ppm of titanium, respectively (see Table 1). The samples were ground to a final thickness of 100 µm by hand using silicon carbide paper of decreasing grain size (P1000 to P4000). Grinding was accomplished equally from both sides of the crystals to expose the central region of the crystal for TEM investigation.

A dimple was ground in the centre of the sample using 6 µm diamond paste leaving a final thickness of approximately 60 µm. The samples were mounted in a standard sample holder made of titanium and were ion-polished at an acceleration voltage of 4 keV (PIPS Model 691, Gatan Inc., USA) until a hole with rims transparent to the electron beam was obtained. Subsequently, ion beam etching was accomplished from both sides.

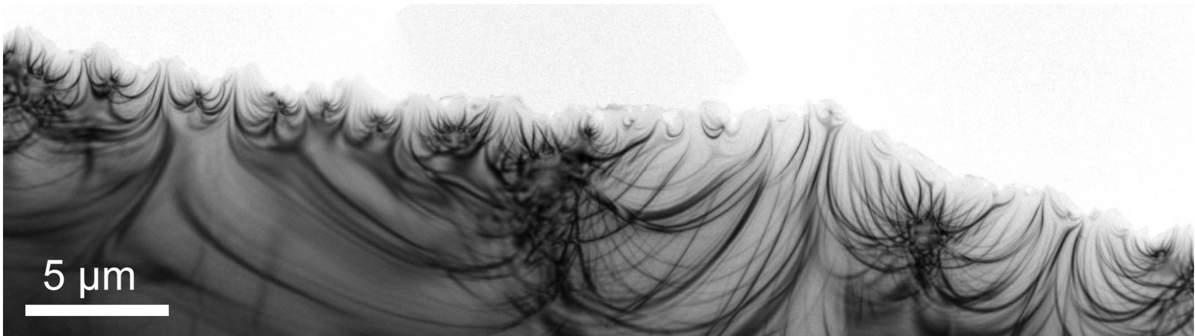

Fig. 1 Rim of the sample containing 1100 ppm of titanium with bending contours, but without extensive precipitation or pronounced dislocation structures.

A Philips Tecnai F30 transmission electron microscope (Philips Electron Optics, The Netherlands) operating at 300 keV was used for the TEM investigations. The system is equipped with a STEM system as well as an EDAX Apollo XLT windowless detector (EDAX Inc., USA). Images were recorded on a bottom-mounted CCD camera (Gatan CCD 694, Gatan Inc., USA). Imaging of the samples was carried out in TEM mode. Image montages of bigger areas were produced with MosaicJ [20], a plugin for the public domain software ImageJ [21].

The samples were exceptionally homogeneous. Along the rim of the holes (see Fig. 1) in the two samples we detected only one possible nanometre sized precipitate, presumable of titanium oxide [22], in an area of several thousand μm^2. Extensive tilting experiments were performed to detect the expected particles by diffraction contrast. During these tilting experiments no indication of dislocation structures could be found. Although this is no proof of the absence of dislocations, which have to be revealed properly by dedicated diffraction contrast imaging, this observation suggests a low dislocation density within the sample.

The dopant level is low for a proper detection by EDS in the transmission electron microscope. Usually, by careful measurement about 5000 ppm of Ti should be detectable. Such concentrations can be reached especially in precipitates or enrichment zones, making EDS analysis possible. Unfortunately, it turned out that the sample holders used for preparation introduced a slight Ti contamination on the sample surface, which rendered EDS analysis unsuitable for detecting low Ti concentrations.

2.3 Diffusion experiments

Thin slices (about 1 mm thick and 15 mm in diameter) were cut from the grown crystal perpendicular to the growth axis (a-axis). These samples were polished to optical flatness with diamond paste of decreasing particle size (15, 6, 3, 1 μm). After ultrasonic cleaning in ethanol the samples were pre-annealed in 200 mbar $^{16}O_2$ gas at 1650 °C for 9 hours to remove polishing damage. The nominally undoped as-grown samples were colourless and remained colourless after pre-annealing. The Ti-doped as-grown samples were light pink with increasing colour intensity as the doping increased. After the pre-annealing step all Ti-doped samples became colourless which indicates that Ti^{3+} oxidised to Ti^{4+} during pre-annealing [23].

A thin layer of $^{26}Al_2O_3$ was deposited on an area of 2×2 mm^2 of the sample surface after pre-annealing. The layer consisted of an approximately homogeneous distribution of small $^{26}Al_2O_3$ particles with a size of about 100 nm. The radioactive isotope ^{26}Al has a half-life time of

7.4×10^5 years which implies a very low specific activity [24]. Details of the deposition technique of ^{26}Al are given elsewhere [25]. To perform a diffusion experiment a sample was placed at room temperature onto the sample holder and moved to the centre of the furnace (see Ref. [10] for a detailed description of the furnace). The furnace tube (single crystalline undoped α-Al_2O_3) was then evacuated to about 10^{-3} mbar total pressure for one hour and was subsequently filled with 180 mbar oxygen gas (which results in a gas pressure of about 200 mbar at annealing temperature). In the next step the furnace was heated at 5 K min^{-1} and then held for annealing time t at the diffusion temperature T. Thereafter the furnace was cooled to room temperature at 5 K min^{-1}.

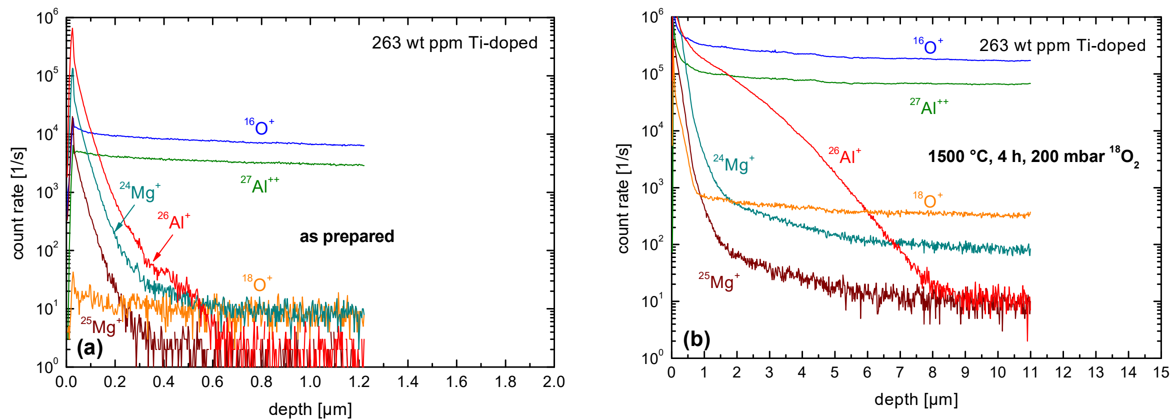

Fig. 2 Typical SIMS depth profiles of an α-Al_2O_3 sample (263 wt ppm Ti-doped) coated with an $^{26}Al_2O_3$ layer: (a) as prepared, (b) after 4 h annealing at 1500 °C in 200 mbar $^{18}O_2$ gas.

Depth distributions of the isotopes ^{26}Al and ^{18}O were determined by Secondary Ion Mass Spectrometry (SIMS) using a Cameca IMS 3f instrument. A 14.5 keV O^- primary beam was applied with a current of about 150 nA and a 50 µm spot size. The raster-scanned area was 250×250 µm^2 and the diameter of the analysed zone was 60 µm. Positive secondary ions were used in the analysis of the samples. Sample charging was prevented by coating the sample surface with a 50 nm thick carbon film.

Typical SIMS raw data of depth profiles measured on the as-prepared and on the annealed samples are shown in Fig. 2. Depth calibration was performed by measuring the SIMS crater depth using a surface profiler (Alpha Step 500, Tencor USA). The depth profiles on the as-prepared surface show high peaks of ^{24}Mg (78.8 % nat. abundance), ^{25}Mg (10.1 % nat. abundance), ^{26}Al (and ^{26}Mg with 11.1 % nat. abundance) near the surface (Fig. 2a). The matrix signals $^{16}O^+$, $^{18}O^+$ and $^{27}Al^{++}$ were also measured to detect any signal drift during the SIMS analysis. The magnesium peaks result from a small amount of magnesium in the ^{26}Al tracer solution [25]. The broadening of the peak signals (^{24}Mg, ^{25}Mg and ^{26}Al) is mainly due to the surface roughness of the $^{26}Al_2O_3$ layer which consists of particles with a size of about 100 nm [25]. Fig. 2b shows depth profiles measured after the diffusion annealing (4 h at 1500 °C in 200 mbar $^{18}O_2$ gas). It can be seen that ^{26}Al can be detected up to a depth of about 8 µm, whereas only a negligibly small amount of ^{18}O diffused into the sample. The magnesium signals (^{24}Mg, ^{25}Mg) show a weakly decreasing slope after 1.5 µm which can be interpreted as the result of a fast diffusion path. However, the volume diffusion coefficient of Mg (verifiable by the tracer isotopes ^{24}Mg and ^{25}Mg) is significantly lower than the volume diffusion coefficient of ^{26}Al so that higher concentrations of Mg remain localized near the surface (below 1.5 µm). This means that the tracer isotopes ^{26}Mg and ^{26}Al were spatially separated by the diffusion process in alumina so that mass 26 can be clearly assigned to ^{26}Al for a depth above 1.5 µm.

To evaluate the diffusion coefficient from the measured depth profiles the solution of the diffusion equation for a constant diffusion source ($c_0 = \text{constant}$) located at $x = 0$ was used [26]

$$c(x) - c_\infty = (c_0 - c_\infty)\,\mathrm{erfc}\left(\frac{x}{L}\right) \quad \text{with} \quad L = 2\sqrt{D \cdot t} \tag{1}$$

where L is the diffusion length, D the diffusion coefficient and t the annealing time at the diffusion temperature. The concentration c_∞ at $x = \infty$ corresponds to the background value of the tracer isotope. As one can see in Fig. 2, there is a background of ^{25}Mg (natural abundance

10.1 %). As ^{26}Mg has nearly the same abundance (11.1 %) c_∞ is due to the mass interference between ^{26}Mg and ^{26}Al, but is virtually zero for ^{26}Al. The applicability of this solution for the granular $^{26}Al_2O_3$ tracer layer was demonstrated elsewhere [25]. For finite heating and cooling rates (5 K min^{-1} in this work) one has to take into account that during heating up/down tracer diffusion already takes place. The procedure to evaluate a corresponding effective additional annealing time is described in detail elsewhere [10].

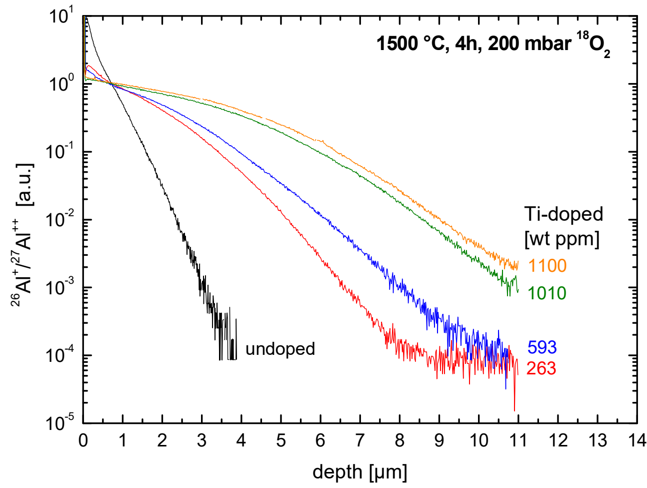

Fig. 3 Comparison of ^{26}Al SIMS depth profiles of five α-Al_2O_3 samples doped with different Ti concentrations (see Table 1). All samples were annealed simultaneously for 4 h at 1500 °C in 200 mbar $^{18}O_2$ gas. In order to improve comparability the SIMS signal ratio $^{26}Al^+/^{27}Al^{++}$ was plotted.

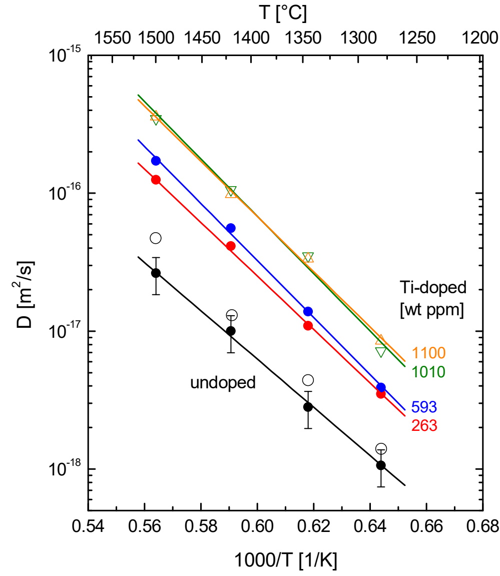

Fig. 4 ^{26}Al diffusion coefficients in nominally undoped and in Ti-doped single crystalline α-Al_2O_3 (see Table 1). The error bars are similar for all measured diffusion coefficients, but are only shown for one data set (undoped α-Al_2O_3) to ensure a clear presentation of all data points. Solid lines are least-squares fits of an Arrhenius relation. Open circles are ^{26}Al diffusion coefficients measured by Fielitz et al. [12] in 2012 in nominally undoped single crystalline α-Al_2O_3.

Table 3 Parameter compilation of the ^{26}Al tracer diffusion experiments performed on α-Al_2O_3 samples with different Ti doping concentrations. D is the ^{26}Al tracer diffusion coefficient and t is the annealing time at diffusion temperature. The diffusion annealing was performed in 200 mbar oxygen gas. $^{18}O_2$ gas (95 % enrichment) was used at 1500 °C, standard oxygen gas ($^{16}O_2$ gas with natural abundance of oxygen isotopes) was used at the other temperatures. The bottom rows comprise the evaluated pre-exponential factors, D_0, and the activation enthalpies, ΔH_a, of the Arrhenius relations (solid lines in Fig. 4).

	undoped		**263 wt ppm Ti**		**593 wt ppm Ti**		**1010 wt ppm Ti**		**1100 wt ppm Ti**	
	t/[h]	D/[m²/s]	t/[h]	D/[m²/s]	t/[h]	D/[m²/s]	t/[h]	D/[m²/s]	t/[h]	D/[m²/s]
1500 °C	4	2.6×10^{-17}	4	1.2×10^{-16}	4	1.7×10^{-16}	4	3.5×10^{-16}	4	3.6×10^{-16}
1420 °C	46	1.0×10^{-17}	6	4.1×10^{-17}	6	5.6×10^{-17}	3	1.1×10^{-16}	3	9.8×10^{-17}
1345 °C	52	2.8×10^{-18}	10	1.1×10^{-17}	10	1.4×10^{-17}	5	3.5×10^{-17}	5	3.3×10^{-17}
1280 °C	72	1.1×10^{-18}	24	3.5×10^{-18}	24	3.9×10^{-18}	8	7.2×10^{-18}	8	8.5×10^{-18}
D_0/[m²/s]	$\left(2.0^{+3.0}_{-1.2}\right)10^{-7}$		$\left(1.1^{+0.9}_{-0.5}\right)10^{-5}$		$\left(8.3^{+11}_{-4.8}\right)10^{-5}$		$\left(2.0^{+11}_{-1.7}\right)10^{-4}$		$\left(7.1^{+12}_{-4.5}\right)10^{-5}$	
ΔH_a/[eV]	3.47 ± 0.3		3.84 ± 0.3		4.09 ± 0.3		4.12 ± 0.3		3.98 ± 0.3	

3 Results

The solubility of TiO_2 is known to be very low and to depend on the chemical potential of oxygen in the ambient atmosphere of the powder mixture where the solid state solution reaction takes place: In air lattice parameter shift could not be used to detect dissolved TiO_2. However, in 1 bar hydrogen at 1500 °C the atomic fraction Ti/Al was determined to be 7.5×10^{-3} [27]. If, as in the present study, the relation between dopant concentration and self-diffusion (of a host element) is investigated the dopant concentration should be less than the dopant solubility. With Ti/Al $< 10^{-3}$ (see Table 1) this requirement is clearly fulfilled in the present work.

In order to demonstrate unambiguously how an increasing Ti concentration affects the Al mobility, five differently doped samples were simultaneously annealed for 4 h at 1500 °C in 200 mbar $^{18}O_2$ gas. This procedure makes sure that the resulting ^{26}Al depth profiles can be directly compared as all the samples had been submitted to exactly identical annealing conditions. Any signal drift during the SIMS analysis can be corrected using the $^{26}Al^{+}/^{27}Al^{++}$ signal ratio. Thus a perfect comparability of the SIMS depth profiles of different samples is obtained. Fig. 3 clearly shows that the Al mobility in α-Al_2O_3 increases with increasing Ti doping concentration. A least-squares fit of equation (1) through the data points of the depth profiles in Fig. 3 yields the ^{26}Al tracer diffusion coefficients at 1500 °C compiled in Table 3 together with the results for the other temperatures.

From Fig. 3 it became obvious that the samples with 263 and 593 wt ppm Ti and the samples with 1010 and 1100 wt ppm Ti had comparable respective Al diffusion coefficients. During the subsequent diffusion annealing at lower temperatures, therefore, these samples were also annealed simultaneously in 200 mbar $^{16}O_2$ gas (compare annealing times in Table 3). The measured ^{26}Al diffusion coefficients in nominally undoped and in Ti-doped α-Al_2O_3 are plotted in Fig. 4. A least-squares fit of an Arrhenius relation yields the pre-exponential factors, D_0, and the activation enthalpies, ΔH_a, compiled in the bottom rows of Table 3.

4 Discussion

Summarising, the key results of this study are:

(I) The Al diffusivity increases with the Ti concentration (see Fig. 4). The activation energy of the Al diffusivity is about (4.0 ± 0.3) eV in the Ti-doped single crystals (see Table 3). In our previous work (3.9 ± 0.3) eV was measured for a Ti concentration of about 300 wt ppm [10].

(II) The activation energy of the Al diffusivity in the undoped single crystal is (3.5 ± 0.3) eV (see Table 3). In our previous work we measured (3.75 ± 0.1) eV [12].

This means that there is no significant difference between the activation energy of the Al diffusion in the Ti-doped and in the undoped samples.

4.1 Ti-doped samples

The samples in the present study are single crystals grown under strongly reducing conditions ($a_{O_2} \approx 10^{-6}$) and contain titanium as Ti^{3+} ions, and probably on Al sites, i.e. $Ti_{Al}^{\times}$ (see section 2.1 above for details) which oxidised almost completely to $Ti_{Al}^{\bullet}$ during pre-annealing at p_{O_2} = 200 mbar [11], which means

$$\left[Ti_{Al}^{\bullet}\right] \approx \left[Ti\right]_{total} = \left[Ti_{Al}^{\bullet}\right] + \left[Ti_{Al}^{\times}\right] \tag{2}$$

where $\left[Ti\right]_{total}$ is the total concentration of Ti in the samples. The respective redox equilibrium reads (after [11])

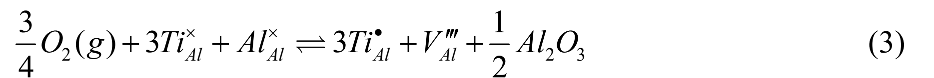

$$\frac{3}{4} O_2(g) + 3Ti_{Al}^{\times} + Al_{Al}^{\times} \rightleftharpoons 3Ti_{Al}^{\bullet} + V_{Al}''' + \frac{1}{2} Al_2O_3 \tag{3}$$

In accordance with the conductivity measurements of Mohapatra and Kröger [11] and a first-principles study of defect energetics in titanium-doped alumina [28] Fielitz et al. [10] assumed that tetravalent titanium ions, Ti^{4+}, occupy aluminium sites and that Al vacancies, V_{Al}''', rather

than oxygen interstitials, O_i'', are the conjugate majority defects, which yields the simple relation $[Ti_{Al}^{\bullet}] = 3[V_{Al}''']$ if defect clustering can be neglected.

In Fig. 5 the ^{26}Al tracer diffusivity, D_{Al}, is plotted as a function of the total Ti concentration (263 wt ppm ≤ c_{Ti} ≤ 1100 wt ppm) in the temperature range 1280 °C ≤ T ≤ 1500 °C with p_{O_2} = 200 mbar. The diagram also contains the D_{Al} data for nominally undoped alumina for the same T, p_{O_2} conditions. The quantitative relation reads

$$D_{Al} \sim [V_{Al}'''] \sim [Ti]_{total}^{n(T)} \tag{4}$$

with $n(T) = 0.55 \cdots 0.77$ increasing with temperature. The interpretation of this result is based on the assumption that the high temperature situation described by equation (2) continues to be valid during the diffusion runs at lower temperatures.

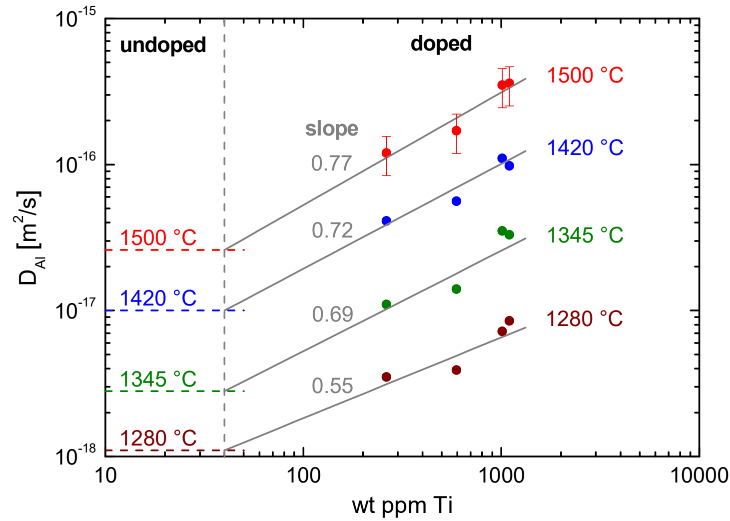

Fig. 5 ^{26}Al diffusion coefficients (solid points) from Fig. 4 are plotted versus the total Ti concentration, $[Ti]_{total}$. The coloured dashed horizontal lines on the left hand side of the diagram correspond to ^{26}Al diffusion coefficients of nominally undoped samples at the given temperatures. The grey lines (with the indicated slopes 0.55 to 0.77) comprise the data for both the doped and the nominally undoped samples at the respective temperatures. The error bars are similar for all measured diffusion

coefficients, but are only shown for one data set (1500 °C) to ensure a clear presentation of all data points.

Table 4 Mott-Littleton-based (M.-L.) and DFT-based calculations of the binding energy of plausible clusters formed as a consequence of the solution of TiO_2. Columns on the right hand side show the mean value of the literature data and the binding energies determined in this work (see text).

Cluster	Binding energy (eV)						
	M.-L.	DFT	DFT	DFT	DFT	Mean value	This work
$\{Ti_{Al}^{\bullet}:V_{Al}'''\}''$	1.95 [29]	1.15 [30]	1.13 [31]	0.85 [28]	1.18 [32]	1.25	1.36
$\{2Ti_{Al}^{\bullet}:V_{Al}'''\}'$	2.88 [29]	1.30 [30]	2.37 [31]	-	-	2.18	2.02
$\{3Ti_{Al}^{\bullet}:V_{Al}'''\}^{\times}$	5.03 [29]	2.93 [30]	2.51 [31]	5.8 [33]	-	4.07	3.52

To explain the temperature dependence of the exponent $n(T)$ in equation (4) we assume that, with decreasing temperatures, for a given Ti concentration an increasing fraction of the mobile aluminium vacancies, V_{Al}''', is bound in (generic) $Ti_{Al}^{\bullet}:V_{Al}'''$ clusters. These (bound) vacancies will not generally contribute to the aluminium transport, which results in a deviation from a temperature independent proportionality between Ti concentration and aluminium diffusivity. Table 4 compiles binding energies of $V_{Al}''':Ti_{Al}^{\bullet}$ clusters provided by Mott-Littleton-based [29] and by DFT-based [28],[30]-[33] simulation calculations. The following possible reaction sequence is most plausible

$$C_1''=\{Ti_{Al}^{\bullet}:V_{Al}'''\}'' \rightleftarrows Ti_{Al}^{\bullet}+V_{Al}''' \qquad (\Delta E_1=1.95\text{ eV}) \tag{5}$$

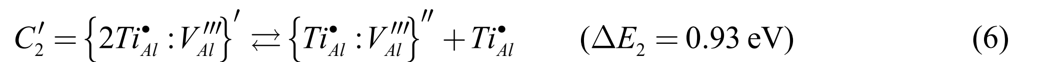

$$C_2'=\{2Ti_{Al}^{\bullet}:V_{Al}'''\}' \rightleftarrows \{Ti_{Al}^{\bullet}:V_{Al}'''\}''+Ti_{Al}^{\bullet} \qquad (\Delta E_2=0.93\text{ eV}) \tag{6}$$

$$C_3^{\times}=\{3Ti_{Al}^{\bullet}:V_{Al}'''\}^{\times} \rightleftarrows \{2Ti_{Al}^{\bullet}:V_{Al}'''\}'+Ti_{Al}^{\bullet} \qquad (\Delta E_3=2.15\text{ eV}) \tag{7}$$

where the ΔE_i values in brackets correspond to the differences of the respective cluster binding energies from reference [29]. The reactions (5) to (7) obey the following mass action relations

$$\left[Ti_{Al}^{\bullet}\right]\left[V_{Al}^{\prime\prime\prime}\right]=K_1\left[C_1^{\prime\prime}\right] \tag{8}$$

$$\left[Ti_{Al}^{\bullet}\right]\left[C_1^{\prime\prime}\right]=K_2\left[C_2^{\prime}\right] \tag{9}$$

$$\left[Ti_{Al}^{\bullet}\right]\left[C_2^{\prime}\right]=K_3\left[C_3^{\times}\right] \tag{10}$$

Charge balance and particle balance result in

$$\left[Ti_{Al}^{\bullet}\right]-3\left[V_{Al}^{\prime\prime\prime}\right]-2\left[C_1^{\prime\prime}\right]-\left[C_2^{\prime}\right]=0 \tag{11}$$

$$\left[Ti_{Al}^{\bullet}\right]+\left[V_{Al}^{\prime\prime\prime}\right]+2\left[C_1^{\prime\prime}\right]+3\left[C_2^{\prime}\right]+4\left[C_3^{\times}\right]=\left[P_{total}\right]=const \tag{12}$$

where $\left[P_{total}\right]$ is the (cumulative) atomic fraction of the point defects ($V_{Al}^{\prime\prime\prime}$ and $Ti_{Al}^{\bullet}$) induced by the Ti doping process. Details on the solution of this system of equations are given in the Appendix.

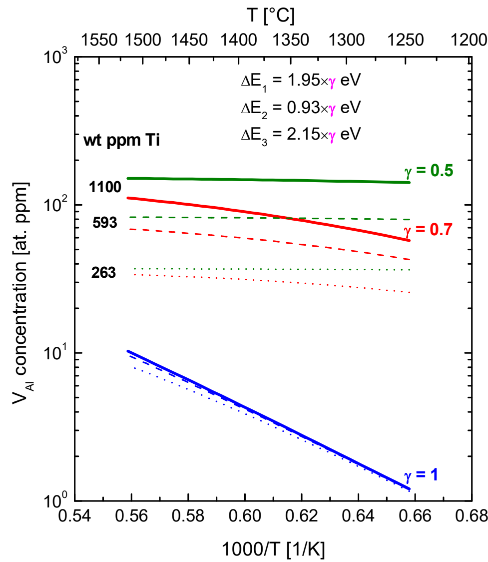

Fig. 6 Calculated aluminium vacancy concentrations vs. reciprocal temperatures for three experimental Ti concentrations and three values of the fit parameter γ of the reaction energies ΔE_i, $i=1,2,3$ according to equation (13).

The binding energies of the clusters or, respectively, the reaction energies, ΔE_i, of the reactions (5)-(7) determine the evolution of the concentrations of the free and the bound defects with temperature and dopant concentration. Theoretically, the three ΔE_i values can be directly determined. Practically, however, even high-quality experimental diffusivity data are not precise enough to allow such a three-dimensional fit procedure. Due to the inherent inaccuracy of the experimental diffusivity data and due to the marked discrepancies of the calculated energies (confer Table 4) a three-dimensional fit procedure had to be replaced by a one-dimensional one. The sole fit parameter γ was defined as follows

$$\Delta E_i(\gamma) = \gamma \times \Delta E_i \quad i = 1 \cdots 3 \tag{13}$$

Considering the marked discrepancies of the DFT-based data the Mott-Littleton-based data set [29] was taken as the starting values ($\gamma = 1$) in the fit procedure to solve the system of equations (8)-(12).

For $\gamma = 1$ one obtains in the whole experimental temperature range (1280 °C ≤ T ≤ 1500 °C) a high fraction of clusters for all Ti concentrations studied in the present work. This leads to a drastically reduced concentration of mobile aluminium vacancies which, moreover, depends strongly on temperatures (see blue curves in Fig. 6). The aluminium vacancy concentration becomes virtually independent of the Ti concentration of the samples. Obviously, lower ΔE_i values have an opposite effect: The green curves in Fig. 6 are calculated for $\gamma = 0.5$. Because of the resulting small values of the reaction energies the fraction of aluminium vacancies does practically not dependent on temperature in the whole range of Ti concentrations, as it is fixed to the highest value possible ($[V_{Al}'''] = [Ti_{Al}^{\bullet}]/3$) given by the electroneutrality condition (11) if clustering is negligible. For $\gamma = 0.7$ one gets an excellent agreement with the experimentally determined concentration dependence of the D_{Al} data. The red curves in Fig. 6 show that the aluminium vacancy concentration is very close to the respective maximum (for each dopant

concentration) at 1500 °C and that the global temperature dependence is not very pronounced (in comparison to the case with $\gamma = 1$).

Fig. 7 shows that with $\gamma = 0.7$ the observed concentration dependence of the aluminium diffusivities in the experimental temperature range and Ti concentration range can be consistently described if the Mott-Littleton-based energies are reduced by 30 %, which yields the following fit values for the three binding energies

$$E_b(C_1'') = 1.37 \text{ eV}; \quad E_b(C_2') = 2.02 \text{ eV}; \quad E_b(C_3^{\times}) = 3.52 \text{ eV} \tag{14}$$

It is certainly only a fortuitous coincidence but, interestingly, the mean values of the calculated cluster binding energies differ by about 8 % from the binding energies determined in the present work for the two charged clusters and by not more than about 16 % for the neutral cluster (see Table 4).

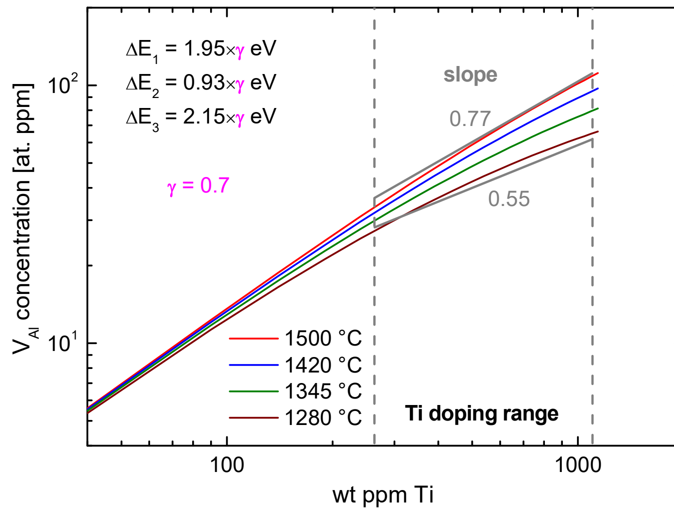

Fig. 7 Numerical simulation of the Ti concentration dependence of the aluminium vacancy concentration in the temperature range 1280 °C ≤ T ≤ 1500 °C. The reaction energies ΔE_i are reduced to 70 % of Mott-Littleton-based energies [29]. The dashed grey vertical lines define the experimental Ti concentration range. The solid grey lines visualise the slopes 0.55 to 0.77 from Fig. 5.

With the three clusters in equation (14) and for the respective binding energies the concentration of the mobile aluminium vacancies is virtually (i.e. considering the error in the activation energies) independent of temperature in the experimental temperature range of the present work for a given Ti concentration. Therefore the experimentally determined activation energy of (4.0 ± 0.3) eV corresponds to the migration energy of the aluminium vacancies and confirms our earlier data ((3.9 ± 0.3) eV in [10] and (3.75 ± 0.1) eV in [12]) as well as a value (3.78 eV) determined from conductivity measurements by Mohapatra and Kröger [11]. These measured migration enthalpies are in good agreement with the isotropic migration energy, 3.8 eV, for V_{Al}''' motion calculated by Dienes et al. [34]. Calculations of Jacobs and Kotomin [35] suggest that the migration energy required for isotropic diffusion in alumina with an Al vacancy mechanism is 3.7 eV.

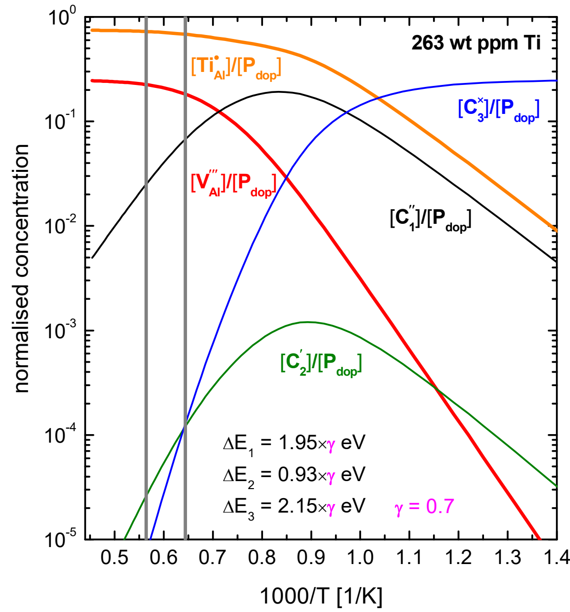

Fig. 8 Numerical simulation of the temperature dependence of normalized concentrations of the point defects V_{Al}''' and $Ti_{Al}^{\bullet}$ and of the clusters C_1'', C_2', $C_3^{\times}$ with $\gamma = 0.7$ for a Ti concentration of 263 wt ppm. The vertical grey straight lines mark the temperature range of the ^{26}Al diffusion experiments of the present study.

In order to get a general view about the temperature dependence of the concentrations of the point defects and the clusters beyond the experimental temperature range of the present study computer simulations have been performed over a larger temperature range for a Ti concentration of 263 wt ppm with the binding energies of equation (14), which are plotted in Fig. 8. The temperature range of the present ^{26}Al diffusion experiments is defined by the vertical solid grey straight lines. In this temperature range the concentrations of the two clusters C_2' and $C_3^{\times}$ (confer equations (6) and (7)) become too low to affect the mobile point defects (V_{Al}''' and $Ti_{Al}^{\bullet}$). As the (normalised) concentration of the cluster C_1'' (see equation (5)) is also in the low percentage range (in the experimental temperature range of the present investigation!) the concentrations of the mobile point defects V_{Al}''' and $Ti_{Al}^{\bullet}$ become almost independent of temperature. With decreasing temperature, however, the concentrations of the clusters increase exponentially. The concentrations of the clusters C_1'' and C_2' go through a maximum before they begin to decrease exponentially with further decreasing temperature. At sufficiently low temperatures the neutral cluster $C_3^{\times}$ is dominant. Because of the high cluster concentration in this temperature range the concentrations of the mobile point defects V_{Al}''' and $Ti_{Al}^{\bullet}$ also decrease exponentially.

Fig. 8 and the foregoing analysis clearly elucidate the physical features of the interaction between mobile and bound defects, which becomes measurable through the experimental determination of the Al diffusivities and the related dopant concentrations.

4.2 Undoped samples

The schematic extrapolation of the aluminium diffusivities obtained for the Ti-doped samples (Fig. 5) suggests for the nominally undoped samples a tetravalent contamination in the order of 40 wt ppm (e.g. of Ti). The GDMS analysis, however, showed that all impurity concentrations are below 3 wt ppm (see Table 2). This means that a potentially induced aluminium vacancy

concentration would be too low by more than a factor of ten in order to affect the aluminium transport. These contradictory experimental findings (GDMS analysis vs. ^{26}Al tracer diffusivity data) suggest the hypothesis that Ti doping induces a change in the aluminium transport mechanism, which is dominant in high-purity undoped single crystals (as in the present study). While the above presented arguments favour (in agreement with literature data) the aluminium transport via (aluminium) vacancies in Ti-doped alumina it cannot be excluded that in nominally undoped crystals aluminium diffuses via an interstitial/interstitialcy mechanism. Interstitial aluminium, $Al_i^{\bullet\bullet\bullet}$, could be induced by the following impurities (see Table 2): Na, K, Ca. Neglecting cluster formation the resulting concentrations of Al interstitials would be around 1 at. ppm. In order to be in agreement with our experimental Al diffusivity data the mobility of the Al interstitials would have to be at least ten times the mobility of the Al vacancies, but with the same migration energy. Fortuitous impurity concentrations and the induced conjugate defect concentrations can vary by orders of magnitude which should consequently also be the case for the measured values of the resulting diffusivities [29],[36]. However, for extremely carefully grown high-purity crystals this conclusion does not seem to hold. This is evident from Fig. 4 where ^{26}Al tracer diffusivities measured on *nominally undoped* samples from the present work are compared to our data measured likewise on nominally undoped crystals in 2012 [12]. Although made by the same crystal grower in our consortium the samples from 2012 and from 2017/18 will definitely not have an absolutely identical crystal growth history. But one does not find significant differences in the respective Al diffusivity data. This contradicts the hypothesis that aluminium transport in nominally undoped high-purity alumina single crystals is exclusively caused by impurities.

Advanced DFT-based calculations favour oxygen vacancies as dominant defects under reducing conditions at equilibrium (!) in the solid (!) (rather than aluminium interstitials) [37]. But the resulting concentrations of the intrinsic defects are many orders of magnitude too low to explain the measured Al diffusivity in undoped crystals. However, a potential induction of

point defects occurs probably during the crystal growth process itself: It seems plausible that at the liquid-solid interface a significant amount of point defects is introduced during the (non-equilibrium!) crystal growth process. Despite minor differences of the growth parameters (e.g. pulling rate, frequency of rotation, geometry of the liquid-solid interface etc.) the concentration of induced defects for different crystal growth runs will, however, most probably be rather similar as the successful growth of high-purity undoped α-Al_2O_3 obeys similar recipes all over the world. Although the following hypothesis of the induction process of defects during the crystal growth procedure is only qualitative it should be considered an alternative way out of a crucial dilemma: The conventional ideas on the induction of point defects rely on the existence of appropriately charged impurities. This concept is, however, no longer valid for sufficiently pure crystals as in the present study.

The following facts support the foregoing hypothesis: During crystal growth the chemical potential of oxygen in the growth unit is low enough to, e.g., reduce Ti^{4+} to Ti^{3+}. Although the oxygen potential for the Ti^{4+}/Ti^{3+} equilibrium is still far off the equilibrium (!) oxygen potential for the (complete) reduction of alumina the resulting chemical potential of aluminium ($\log a_{Al(g)} \approx -8$) at the Al_2O_3(l)/Al_2O_3(s)/(Ar/H_2) triple phase boundary (TBP) will cause a slight substoichiometry of the O/Al ratio of the growing crystal. At the melting point of alumina the calculated Al activity corresponds to an Al vapour pressure of about 10^{-6} mbar [38]. Assuming simple Hertz-Knudsen evaporation kinetics it results that the oxygen evaporation flux is about three orders of magnitude higher than the Al flux. The resulting difference in the local chemical potentials at the TBP will favour a local enrichment of Al due to the disintegration of the surface of the melt, thus leading to an incorporation of Al interstitials plus electrons during solidification according to the following reaction equation

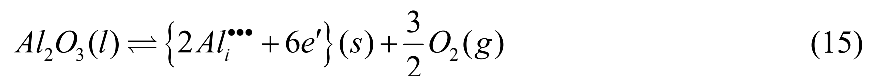

$$Al_2O_3(l) \rightleftharpoons \left\{2Al_i^{\bullet\bullet\bullet} + 6e'\right\}(s) + \frac{3}{2}O_2(g) \qquad (15)$$

From reference [11] it is evident that the ionic and electronic transference numbers are each about 0.5 at 1600 °C for the range of oxygen activities generally occurring in crystal growth units.

5 Conclusions

At the beginning of the discussion section (see section 4) the key results of the present work are listed. The close cooperation with experienced crystal growers has turned out to be crucial as it could be demonstrated unequivocally that the ^{26}Al tracer diffusion increases with the Ti concentration (see Fig. 4). The quantitative relation is, however, more complicated than one would expect from the most probable solution reaction in the absence of clusters and the corresponding electroneutrality condition ($\left[Ti_{Al}^{\bullet}\right]-3\left[V_{Al}'''\right]\cong 0$) [10]: The parameter $n(T)$ of the logarithmic relation (see equation (4)) increases with temperature (see Fig. 5). This temperature dependence can, however, be quantitatively rationalised if the formation of three types of $Ti_{Al}^{\bullet}:V_{Al}'''$ clusters is taken into consideration whose binding energies are obtained from the experimental Al diffusivities with the aid of a phenomenological cluster model.

The conventional explanation of the surprisingly high values of the ^{26}Al tracer diffusion coefficients in nominally undoped crystals (confer Fig. 5) would require a contamination with unintentional tetravalent impurities in the order of 40 wt ppm. Such a high impurity level can, however, be definitely excluded (see Table 2). If the observed aluminium diffusion in the nominally undoped crystals were operating via an interstitial/interstitialcy mechanism due to unintentionally introduced impurities with lower valence (than Al^{3+}) one would expect large variations in the aluminium diffusion data in analogy to the oxygen diffusion data [29],[36]. Because of the extremely high purity of the crystals used in the present work we therefore formulate a new hypothesis in order to propose a physically sound explanation of the astonishingly high values of the ^{26}Al diffusion coefficients in high-purity undoped crystals. This new concept is based on the injection of Al interstitials and electrons into the crystal at the

liquid/solid interface because of the low oxygen potential maintained during the crystal growth process.

Acknowledgements

We are indebted to Dr. Robert A. Jackson and to Professor Yuichi Ikuhara and Professor Katsuyuki Matsunaga for advice on cluster binding energies. We are grateful to Mrs. Angelika Ohlendorf for the careful polishing of α-Al_2O_3 single crystal samples. Financial support from Deutsche Forschungsgemeinschaft (DFG) via the grant FI 881/9-1 is gratefully acknowledged.

Appendix

Solution of the system of equations (8)-(12)

We define the following normalised variables

$$x \equiv \frac{\left[Ti_{Al}^{\bullet}\right]}{\left[P_{total}\right]};\quad y \equiv \frac{\left[V_{Al}'''\right]}{\left[P_{total}\right]};\quad z_1 \equiv \frac{\left[C_1''\right]}{\left[P_{total}\right]};\quad z_2 \equiv \frac{\left[C_2'\right]}{\left[P_{total}\right]};\quad z_3 \equiv \frac{\left[C_3^{\times}\right]}{\left[P_{total}\right]} \tag{A1}$$

and normalised parameters

$$a_1 \equiv \frac{K_1}{\left[P_{total}\right]};\quad a_2 \equiv \frac{K_2}{\left[P_{total}\right]};\quad a_3 \equiv \frac{K_3}{\left[P_{total}\right]} \tag{A2}$$

The normalised parameters a_i are calculated by

$$a_i = \frac{K_i}{\left[P_{total}\right]} = \frac{K_i^0}{\left[P_{total}\right]}\exp\left(-\frac{\Delta E_i}{k_B T}\right) \tag{A3}$$

where k_B is the Boltzmann constant and ΔE_i is presented in equations (5)-(7). Setting generically $\Delta S = 2\,k_B$ in the pre-exponential factor $K_i^0 = \exp\left(\Delta S / k_B\right)$ one gets

$$a_i == \frac{1}{\left[P_{total}\right]}\exp\left(2 - \frac{\Delta E_i}{k_B T}\right) \tag{A4}$$

Equations (8)-(12) now become

$$x\,y = a_1\,z_1;\quad x\,z_1 = a_2\,z_2;\quad x\,z_2 = a_3\,z_3 \tag{A5}$$

$$x - 3y - 2z_1 - z_2 = 0 \quad \text{(A6)}$$

$$x + y + 2z_1 + 3z_2 + 4z_3 = 1 \quad \text{(A7)}$$

This system of equations was solved numerically by the computer algebra system Maple 16 (Waterloo Maple Inc.).

If clustering is negligible ($z_i \to 0$) equations (A6) and (A7) simplify

$$x - 3y = 0; \quad x + y = 1 \quad \text{(A8)}$$

with the solution

$$x = \frac{[Ti_{Al}^{\bullet}]}{[P_{total}]} = \frac{3}{4}; \quad y = \frac{[V_{Al}^{\prime\prime\prime}]}{[P_{total}]} = \frac{1}{4} \quad \text{(A9)}$$

Because in this case the fraction of clustered Ti ions is negligible one can conclude

$$[P_{total}] = \frac{4}{3}[Ti_{Al}^{\bullet}]_{total} = \frac{4}{3}C_{at.}^{Ti} \quad \text{(A10)}$$

where $[Ti_{Al}^{\bullet}]_{total} = C_{at.}^{Ti}$ is the atomic fraction of the dopant Ti. The relation between the atomic fraction and the weight fraction, C_{wt}^{Ti}, is

$$C_{at.}^{Ti} = \frac{2M_{Al} + 3M_O}{5M_{Ti}} C_{wt}^{Ti} = 0.426 \times C_{wt}^{Ti} \quad \text{(A11)}$$

where M_i is the corresponding molar mass. Combining equations (A10) and (A11) one gets

$$[P_{total}] = 0.568 \times C_{wt}^{Ti} \quad \text{(A12)}$$

This relation was used to calculate $[P_{total}]$ from Ti doping concentrations measured by weight fractions.

References

[1] R. Prescott, M.J. Graham, The formation of aluminum oxide scales on high-temperature alloys, Oxid. Met. 38 (1992) 233–254.

[2] A.H. Heuer, D.B. Hovis, J.L. Smialek, B. Gleeson, Alumina Scale Formation: A New Perspective, J. Am. Ceram. Soc. 94 (2011) s146–s153.

[3] J.H. Harding, K.J.W. Atkinson, R.W. Grimes, Experiment and Theory of Diffusion in Alumina, J. Am. Ceram. Soc. 86 (2003) 554–559.

[4] R.H. Doremus, Diffusion in alumina, J. Appl. Phys. 100 (2006) 101301-1–17.

[5] A.H. Heuer, T. Nakagawa, M.Z. Azar, D.B. Hovis, J.L. Smialek, B. Gleeson, N.D.M. Hine, H. Guhl, H.-S. Lee, P. Tangney, W.M.C. Foulkes, M.W. Finnis, On the growth of Al_2O_3 scales, Acta Mater. 61 (2013) 6670–6683.

[6] M. Le Gall, B. Lesage, J. Bernardini, Self-diffusion in α-Al_2O_3 I. Aluminium diffusion in single crystals, Phil. Mag. A 70 (1994) 761–773.

[7] P. Fielitz, G. Borchardt, M. Schmücker, H. Schneider, Al-26 diffusion measurement in 2/1-mullite by means of Secondary Ion Mass Spectrometry, Solid State Ionics 177 (2006) 493–496.

[8] P. Fielitz, G. Borchardt, Self-Diffusion of the Constituent Elements in Alpha-Alumina, Mullite and Aluminosilicate Glasses, Diffusion Foundations Vol. 8, Progress in Thermodynamics, Diffusion, Ion and Proton Transport of Ionic Compounds and Ion-Conducting Polymer Films, Editor H. Mehrer, Trans Tech Publications (2016), p. 80.

[9] A.E. Paladino, W.D. Kingery, Aluminum Ion Diffusion in Aluminum Oxide, J. Chem. Phys. 37 (1962) 957–962.

[10] P. Fielitz, G. Borchardt, S. Ganschow, R. Bertram, A. Markwitz, ^{26}Al tracer diffusion in titanium doped single crystalline α-Al_2O_3, Solid State Ionics 179 (2008) 373–379.

[11] S.K. Mohapatra, F.A. Kröger, Defect Structure of α-Al_2O_3 Doped with Titanium, J. Am. Ceram. Soc. 60 (1977) 381–387.

[12] P. Fielitz, G. Borchardt, S. Ganschow, R. Bertram, ^{26}Al tracer diffusion in nominally undoped single crystalline α-Al_2O_3, Defect and Diffusion Forum Vols. 323-325 (2012) 75–79.

[13] P. Lacovara, L. Esterowitz, M. Kokta, Growth, spectroscopy, and lasing of titanium-doped sapphire, IEEE J. Quantum Electr. 21 (1985) 1614–1618.

[14] A. Sanchez, A.J. Strauss, R.L. Aggarwal, R.E. Fahey, Crystal growth, spectroscopy, and laser characteristics of Ti:Al_2O_3, IEEE J. Quantum Electr. 24 (1988) 995–1002.

[15] R. Uecker, D. Klimm, S. Ganschow, P. Reiche, R. Bertram, M. Roßberg, R. Fornari, Czochralski growth of Ti:sapphire laser crystals, Proc. SPIE 5990, Optically Based Materials and Optically Based Biological and Chemical Sensing for Defence II, 599006 (15 October 2005).

[16] S. Ganschow, D. Klimm, R. Bertram, On the effect of oxygen partial pressure on the chromium distribution coefficient in melt-grown ruby crystals, J. Crystal Growth 325 (2011) 81–84.

[17] A. Nehari, A. Brenier, G. Panzer, K. Lebbou, J. Godfroy, S. Labor, H. Legal, G. Chériaux, J.P. Chambaret, T. Duffar, R. Moncorgé, Ti-Doped Sapphire (Al_2O_3) Single Crystals Grown by the Kyropoulos Technique and Optical Characterizations, Crystal Growth & Design 11 (2011) 445–448.

[18] R. Bertram, M. Böck, Zerkleinerung von Saphir-Kristallen zur chemischen Analyse, Chem. Ing. Technik 77 (2005) 1965–1969.

[19] V.D. Kurochkin, L.P. Kravchenko, Analysis of impurities in high-purity aluminum oxide by glow discharge mass spectrometry, Powder Metall. Met. Ceram. 45 (2006) 493–499.

[20] P. Thévenaz, M. Unser, User-Friendly Semiautomated Assembly of Accurate Image Mosaics in Microscopy, Microscopy Research and Technique 70 (2007) 135–146.

[21] C.A. Schneider, W.S. Rasband, K.W. Eliceiri, NIH Image to ImageJ: 25 years of image analysis, Nature methods 9 (2012) 671–675.

[22] J. He, K.P.D. Lagerlöf, A.H. Heuer, Structural evolution of TiO_2 Precipitates in Ti-doped Sapphire (α-Al_2O_3), J. Am. Ceram. Soc. 94 (2011) 1272–1280.

[23] G.A. Keig, Influence of the valence state of added impurity ions on the observed color in doped aluminum oxide single crystals, J. Cryst Growth 2 (1968) 356–360.

[24] J.M. Ferguson, Al^{26} Decay Scheme, Phys. Rev. 112 (1958) 1238 –1240.

[25] P. Fielitz, G. Borchardt, M. Schmücker, H. Schneider, Al-26 diffusion measurement in 2/1-mullite by means of Secondary Ion Mass Spectrometry, Solid State Ionics 177 (2006) 493–496.

[26] J. Crank, The Mathematics of Diffusion, 2nd ed., Oxford Univ. Press, Oxford 1975.

[27] A.R. Moon, M.R. Phillips, Defect clustering in H,Ti:α-Al_2O_3, J. Phys. Chem. Solids 52 (1991) 1087–1099.

[28] K. Matsunaga, A. Nakamura, T. Yamamoto, Y. Ikuhara, First-principles study of defect energetics in titanium-doped alumina, Phys. Rev. B 68 (2003), 214102-1–8.

[29] K.P.D Lagerlöf, R.W. Grimes, The defect chemistry of sapphire (α-Al_2O_3), Acta mater. 46 (1998) 5689–5700.

[30] L.Yu. Kravchenko, D.V. Fil, Defect complexes in Ti-doped sapphire: A first principles study, J. Appl. Phys. 123 (2018) 023104-1–11.

[31] K. Frensch, Ab initio studies of defect concentrations and diffusion in metal oxides, Thesis, Imperial College London, 2011, DOI: 10.25560/7111

[32] K. Matsunaga, T. Mizoguchi, A. Nakamura, T. Yamamoto, Y. Ikuhara, Formation of titanium-solute clusters in alumina: A first-principles study, Appl. Phys. Lett. 84 (2004) 4795–4797.

[33] K. Matsunaga, Y. Ikuhara: personal communication (March 2020)

[34] G.J. Dienes, D.O. Welch, C.R. Fischer, R.D. Hatcher, O. Lazareth, M. Samberg, Shell-model calculation of some point-defect properties in α-Al_2O_3, Phys. Rev. B 11 (1975) 3060–3070.

[35] P.W.M. Jacobs, E. Kotomin, Defect energies for pure corundum and for corundum doped with transition metal ions, Philos. Mag. 68 (1993) 695–709.

[36] K.P.D. Lagerlöf, T.E. Mitchell, A.H. Heuer, Lattice Diffusion Kinetics in Undoped and Impurity-Doped Sapphire (α-Al_2O_3): A Dislocation Loop Annealing Study, J. Am. Ceram. Soc. 72 (1989) 2159–2171.

[37] N.D.M. Hine, K. Frensch, W.M.C. Foulkes, M.W. Finnis, Supercell size scaling of density functional theory formation energies of charged defects, Phys. Rev. B 79 (2009) 024112–1-13.

[38] I. Barin, O. Knacke, O. Kubaschewski, Thermochemical Properties of Inorganic Substances (Supplement), Springer, Berlin 1977.